Impedance-matching anode for fast timing signals

Peter Wurz and Lukas Gubler
Physikalisches Institut, Universität Bern, Sidlerstrasse 5, 3012 Bern, Switzerland

(Received 11 October 1993; accepted for publication 5 January 1994)

In this article a novel design for signal anodes for ultrafast microchannel plate detectors is introduced. A detector assembly was designed and built with an impedance-matched transition line (50 Ω line resistance) from anode to cable connector which is considerably smaller than other, commercially available, solutions and at the same time has about four times the active area with no limitations for up scaling to even larger active areas. Theoretical proof is given that the impedance matching can be achieved over the entire transition line. The design makes use of a bipolar geometry and is flexible to accommodate differing experimental needs. The design was chosen to optimize for small overall size with good temporal response at the same time. The detector was tested with an alpha particle source and an excellent time response was obtained. Although the design was driven by special needs for space application the detector can be applied wherever short timing pulses are needed.

I. INTRODUCTION

At our institute we develop and build mass spectrometers to characterize plasma distributions in extraterrestrial space. Since these instruments are flown on satellites or spacecraft, there are very exacting requirements concerning their size, weight, and performance. Only small, sophisticated devices can succeed. In the energy range of 1 keV/nucleon to 1 MeV/nucleon the current generation of instruments is based on the time-of-flight (TOF) technique for mass identification.[1] The ions to be analyzed with these instruments enter a TOF section by passing through a thin carbon foil ($\approx$100 Å thickness). Thereby, electrons are released from the carbon foil which trigger the time measurement. At the end of the TOF section the ions hit another detector which produces the stop signal for the TOF measurement. In these instruments, also called linear TOF mass spectrometers, the resolution is ultimately limited to $m/\Delta m \approx 30$ due to straggling and scattering of particles in the carbon foil. A new generation of TOF mass spectrometers alleviates this problem by having the ions travel in a suitably configured electric field which compensates for the above-mentioned effects. With the latter instruments, which are called isochronous TOF mass spectrometers,[2–4] mass resolutions of $m/\Delta m$ up to 100 are obtained,[5] determined by the uncertainties of the time measurement and by imperfections in the realization of the electric field (which is a minor problem). In order to maximize the sensitivity of these instruments, detectors with large active areas are used. To meet the requirements concerning weight, active area, and timing accuracy, microchannel plates (MCP) are the best and probably the only choice as particle detectors.

Usually, in a linear as well as in an isochronous instrument the TOF to be measured ranges from nanoseconds to several hundred nanoseconds, depending on the energy and kind of particle to be analyzed. Especially for isochronous instruments, the time resolution has to be better than 1 ns to obtain good mass resolution. There are several reasons why the time interval between the start and stop pulse is small in instruments for space application:

(1) There is limited weight and space available on a spacecraft, which limits the size of the instrument and ultimately results in a short flight path.
(2) The particles must be accelerated to relatively high kinetic energies in order to utilize the carbon-foil technique. Approximately a minimum kinetic energy around 1 keV/amu is needed to pass the entrance foil and release electrons with sufficient probability.[6,7]
(3) Only one ion is analyzed at a time. Thus, a shorter TOF results in a smaller dead time of the sensor and therefore, the instrument is capable of a higher maximum count rate and higher dynamic range.

The maximum achievable time resolution is limited by the inherent transient time spread of the charge pulse produced by the MCPs, given by the electron multiplication process inside the MCPs. For accurate time measurements a fast rise time of the output pulse is desired. The shortest pulse width of existing systems is somewhat below a nanosecond.[8–10] Obviously, one of the critical components is the anode that picks up the signal from the back side of the second channel plate and feeds it into the transmission line. To operate the detector at optimal conditions, the electronic pickup and transmission system must have a line impedance of 50 Ω to couple the pulses to a standard transmission line with minimal reflections.

To sum up our design goals, we wanted to develop a MCP-detector assembly to meet the following requirements: it should be small in size and weight, but with large active area and strictly a 50 Ω line impedance from the anode front surface to vacuum feedthrough for short signal pulses.

II. THEORY

A flat anode is the most widely used geometry for signal pickup from MCPs. If no precautions are taken for

 0034-6748/94/65(4)/871/6/$6.00

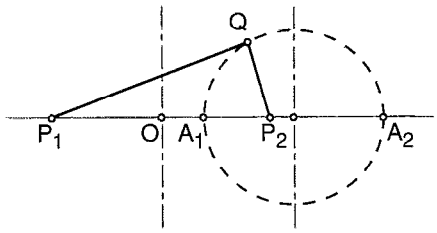

FIG. 1. Geometric principle of the circle of Apollonius (dashed line) for the two points P_1 and P_2.

impedance matching, a coaxial cable is simply attached to the anode to read out the signal. If one is concerned with the temporal performance of the signal readout, more sophistication in the signal transmission from the anode to the 50 Ω cable is needed. Basically, one has to design a way to connect a thick coaxial transmission line, given by the active area of the MCP, to a regular signal cable, which is of much smaller diameter at constant impedance throughout. The impedance Z_L of a coaxial transmission line is given by[11]

$$Z_L=\sqrt{\frac{\mu_0}{\epsilon_0}}\frac{1}{2\pi\sqrt{\epsilon_r}}\log\left(\frac{D}{d}\right) \quad \text{with} \quad \frac{1}{2\pi}\sqrt{\frac{\mu_0}{\epsilon_0}}=60\ \Omega, \tag{1}$$

where d is the inner and D the outer diameter of the coaxial line, ϵ_r is the relative dielectric constant, ϵ_0 is the vacuum dielectric constant, and μ_0 is the vacuum permeability. Given the dielectric material, the impedance is only governed by the ratio of the inner and the outer diameter of the transmission line. The simplest way to match two coaxial transmission lines with different diameters (however same ratios D/d) is the use of a step transition.[12] Thereby an unsteadiness in the form of a longitudinal capacitance is introduced where signal reflections and distortions are introduced. The step transition works well if the step size is small compared to the wavelength of the signal, which is not the case in our application. A better solution to this problem is the well-known cone line.[10,13] A cone line uses two concentric cones with a common tip. With the cones, unsteadinesses are only introduced at the ends of the transition line where the cone yields into the straight line. These unsteadinesses can be minimized by using small opening angles of the cones; however, this lengthens the transition line significantly. Usually the cone length is at least twice the anode diameter. This causes additional weight and bulkiness and poses serious drawbacks for our application, especially with the large active area detectors we have to use.

The concept for the transition line is based on the circle of Apollonius (Apollonius of Perga, circa 262 to 190 B.C.) which is illustrated in Fig. 1. The circle of Apollonius is the locus of points Q, where the ratio of the distances between any point on the circle and two points P_1 and P_2 is constant[14]

$$\frac{\overline{QP_1}}{\overline{QP_2}}=\text{const}\,\forall Q \quad \text{if} \quad \overline{OP_1}^2=\overline{OP_2}^2=\overline{OA}_1\cdot\overline{OA}_2. \tag{2}$$

For the inner and outer electrode we employ two different circles of Apollonius for the same two points P (due to the symmetry regarding O we will just use the symbol P for both points instead of P_1 and P_2 from now on). The two circles of Apollonius are members of a nonintersecting pencil of coaxial circles and are defined by

$$\overline{OP}^2=\overline{OA}\cdot\overline{OB}=\overline{OC}\cdot\overline{OD}, \tag{3}$$

with O the origin of the pencil of coaxial circles, the two points P on each side of the origin, and A, B, C, and D the points of intersection of the line OP (x axis in our case) with the two circles of Apollonius. Orthogonal to this nonintersecting pencil of coaxial circles there is an intersecting pencil of coaxial circles. All of the latter circles go through the points P and are defined by

$$\overline{OP}^2=-\overline{OA^*}\cdot\overline{OB^*}=-\overline{OC^*}\cdot\overline{OD^*}, \tag{4}$$

where A^*, B^*, C^*, and D^* are the intersections of two circles with a line through the origin O that is perpendicular to the line OP (y axis in our case). Together, the two pencils of coaxial circles form a coordinate system in bipolar geometry. The advantage of using a bipolar geometry is that the nonintersecting and the intersecting pencils of coaxial circles directly represent the electric potential and field lines. This was verified by numerical field calculations.

To obtain a complete transition line in bipolar geometry we have to use two sets of the above-defined orthogonal families of circles; one for the anode side and one for the cable side of the transition. These two sets have to be fitted together adequately to maintain constant impedance over the transition line. In mathematical terms, a nonintersecting pencil of coaxial circles is fitted to an intersecting pencil of coaxial circles, with the origin displaced along the y axis for the latter. We show in the Appendix A that the impedance is indeed constant along the entire transition line. In a similar way, a geometry based on the circle of Apollonius has been applied successfully to connect a cable to a double-conical antenna.[15] In contrast to the earlier design, we have to use two sets of these families of circles to obtain a complete transition line in bipolar geometry.

Therefore, in our design the inner and outer conductors of the transition line have the shape of circles, rotated around the central axis of the transmission line. The schematics of the design are depicted in Fig. 2. The origins of the two sets of families of circles are separated by a distance h, which gives the length of the transition line. Choosing r_1' and r_1'', we get for the length of the transition line

$$h=(C''-C')\sqrt{\frac{2(r_1'+r_1'')}{C''-C'}-1}, \tag{5}$$

whereby we simplified our notation in the following way: we measure all distances to the origin O' and write A' for the distance $\overline{O'A'}$, A'' for $\overline{O''A''}$, and so forth. The radii (r_1', r_1'',...) are measured as depicted in Fig. 2. A pair of circles in this geometry is defined by A', C', and r_1', or by A'', C'', and r_1'', where the single prime denotes the cable side and the double prime denotes the anode side of the

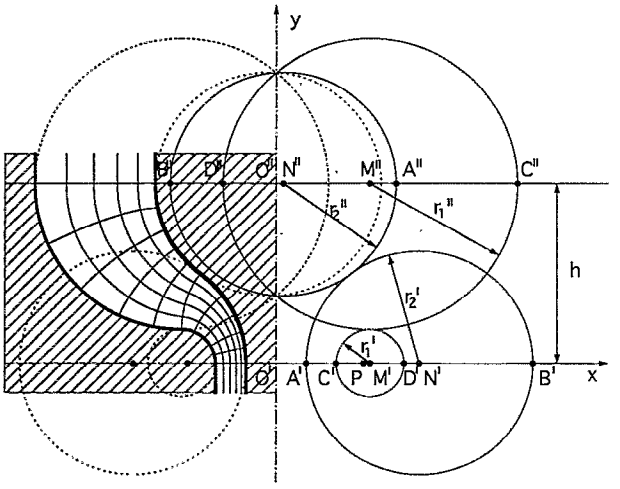

FIG. 2. Schematic drawing showing the cross section of the transition line. The circles on the anode (top plane) and the cable side (bottom plane) are both from a family of circles in bipolar geometry.

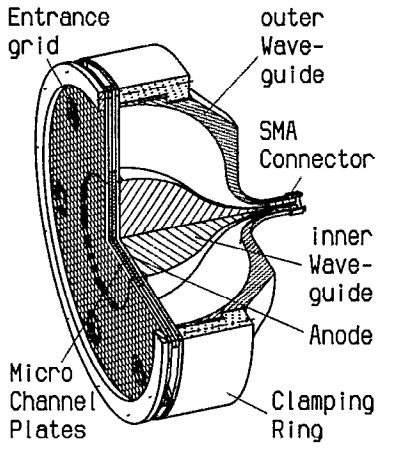

FIG. 3. Cut-through image of the actual design of the channel plate assembly. The 50 Ω anode with the transition line in bipolar geometry yields directly into a standard high-frequency connector (SMA-type).

transition line. C' is the outer diameter of the cable and A'' is given by the active area of the MCP. A' and C'' are then derived from Eq. (1). Thus, A', A'', C', and C'' are given by the dimension and impedance of the transition line; r_1' and r_1'' can be chosen freely. It can be easily verified that all other geometrical dimensions follow from Eqs. (3) and (4). At the cable side of the transition line we have

$$M'=C'+r_1', \tag{6}$$

$$N'=\frac{C'(C'+2r_1')+A'^2}{2A'}, \tag{7}$$

$$r_2'=\frac{C'(C'+2r_1')-A'^2}{2A'}, \tag{8}$$

$$P'=\sqrt{C'(C'+2r_2')}, \tag{9}$$

and at the anode side of the transition line we have

$$M''=C''-r_2'', \tag{10}$$

$$N''=\frac{A''^2+C''(C''-2r_1'')}{2A''}, \tag{11}$$

$$r_2''=\frac{A''^2-C''(C''-2r_2'')}{2A''}, \tag{12}$$

$$P''=\sqrt{-C''(C''-2r_1'')}. \tag{13}$$

Equations (6)–(13) are sufficient to design a transition line. To optimize the transition line with respect to the above-mentioned criteria, we make two additional choices. These are

(1) To obtain the smallest reasonable length of the transition line we chose the circles given by r_1' and r_1'' to have horizontal tangents at the point T_1, which is where they connect (i.e., $M'=M''$). This reduces Eq. (5) to

$$h=(C''-C'). \tag{14}$$

(2) For best signal propagation the curvature on the inner conductor is made minimal over the length of the transition line, which results in $r_2'=r_2''$. From that we get for r_1'

$$r_1'=\frac{A'}{4C'}(A''+A')+\frac{1}{4}(C''-3C') \tag{15}$$

and for r_1''

$$r_1''=C''-C'-r_1'. \tag{16}$$

Thus, the length of the transition line, h, is basically equal to the diameter of the active area of the MCP. This design is substantially smaller than a cone-shaped transition line, at least by a factor of 2. Although we made some specific choices for h, r_1', and r_1'', any set of these parameters will give a transition line with constant impedance as is shown in Appendix A, as long as Eqs. (3)–(13) are fulfilled. Thus, many different shapes of the transition line can be realized, like very elongated units close to a cone line or very short units. We chose to optimize the design for small overall size with good temporal response at the same time.

III. DESIGN AND MEASUREMENTS

The dimensions of the transition line are designed using the formulas given above. The outside of the detector assembly is optimized for minimum weight. The transition line directly yields into the output connector without any adapter piece in between. A SMA-type connector is used, which is standard for high-frequency applications. The channel plates have been purchased from Galileo (type 1330-3320, nonimaging quality). They have an active area of 40 mm diam and are mounted in a Chevron configuration. An electric field is applied between the channel plates to accelerate the electrons coming out of the first channel

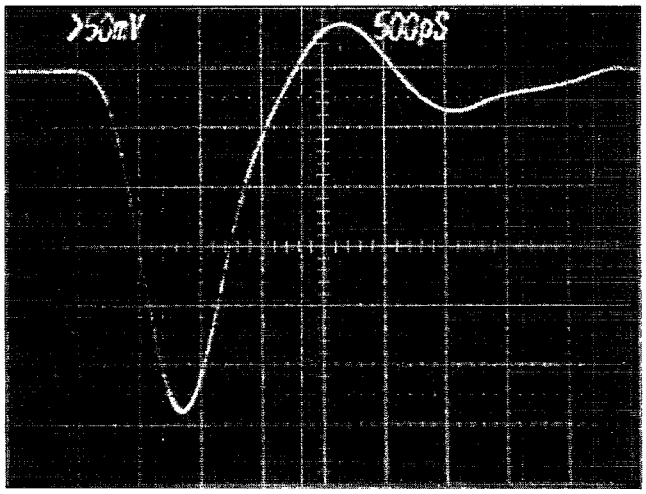

FIG. 4. Oscilloscope trace of a detector output pulse.

plate, which significantly shortens the width of the output pulse.[10] A drawing of the actual detector design is shown in Fig. 3.

Only materials compatible with an ultrahigh-vacuum (UHV) environment are used for the detector: The transition line, that is the outer and inner waveguide, is made out of aluminum and plated with gold to give low surface resistance; the channel plates are held with ceramic fixtures; and all electrical contacts are made through metalized polyimide foils. The clamping ring is made out of polyetherimide. An etched gold grid (92% transmission) terminates the detector at the entrance side. In the design, great care has been taken that the detector has good outgassing capabilities, which do not interfere with the electrical properties.

So far the entire transition from the anode to the connector is made in vacuum. However, at the connector side a dielectric material is used to hold the inner conductor in place. Therefore, a suitable transition from a vacuum line to a coaxial line filled with a dielectric material has to be found. One way to accommodate a changing dielectric constant along a transmission line is to minimize signal reflections by using the "Brewster angle" effect.[16] Although this effect is only valid in an approximate way for coaxial lines, good results have been achieved.[16] Since we wanted to build this transition without changing the outer diameter of the line, we had to use a different approach for this transition. Formulas to calculate the shape of the transition from a vacuum line to a coaxial line filled with a dielectric material are given in the Appendix B together with a schematic drawing (Fig. 6).

The measurements were performed in a vacuum chamber with a base pressure around 10^{-7} mbar. The radiation source was an alpha particle source (Americium) with an intensity of $\approx 10^3$ Bq. Inside the vacuum, the signal output of the detector was connected to an UHV feedthrough (50 Ω SMA-type) by a 1 m cable. The output pulses were recorded directly with a Tektronix oscilloscope (model 7104) with a bandwidth of 1 GHz and a rise time of 350 ps. Figure 4 shows a typical output pulse of the detector. As can be seen from that figure, the measured rise time is 450 ps and the pulse width is 750 ps, with no corrections applied to account for the bandwidth of the measuring electronics. A fluctuation of the measured rise time of less than ±10% is observed. Since we illuminated the entire active area of the detector during the measurements the fluctuation of the temporal response could be caused by different rise times for different impact positions on the active area of the detector. However, given the magnitude of the effect we conclude that the temporal response is not

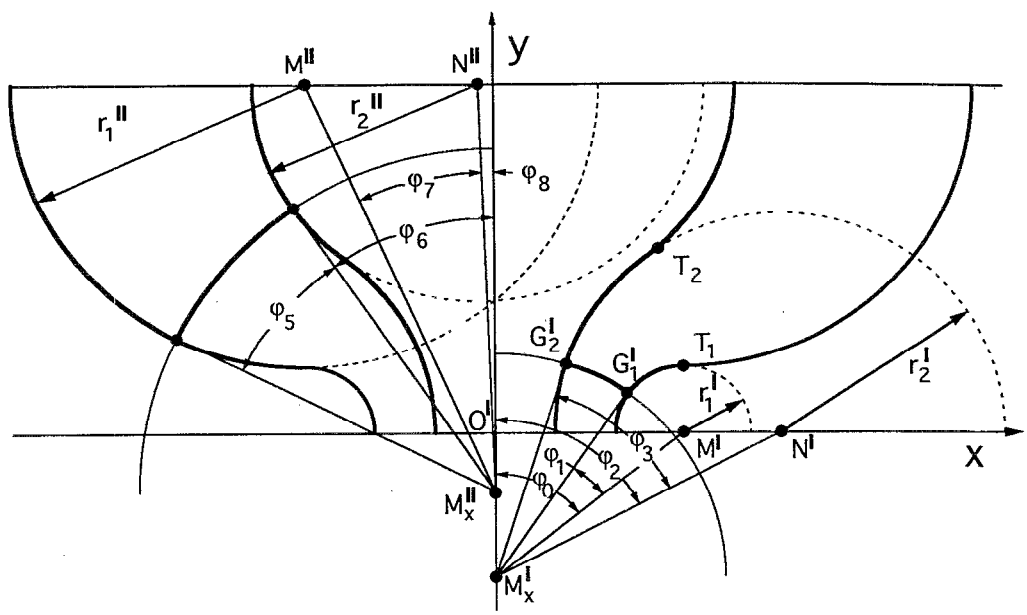

FIG. 5. Schematic drawing of the transition line showing the origin of the circles of the field lines and the limits of integration.

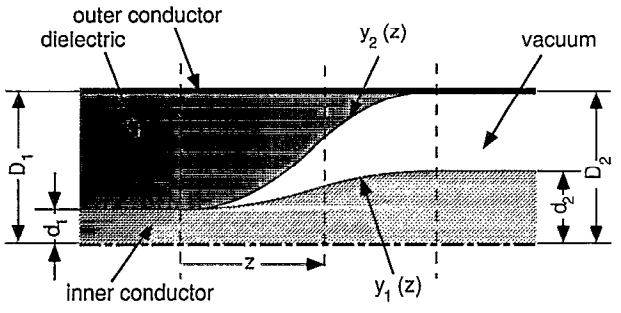

FIG. 6. Schematics of the transition from a coaxial line in vacuum (right side) to a coaxial line filled with a dielectric medium (left side).

(or rather limited) sensitive to the impact position. Performing a first-order correction of the measured detector response results in a *true* rise time of 280 ps. However, since the electronic circuitry following the detector output will not be much faster than 1 GHz the measured value of the rise time has more significance. In a detailed theoretical investigation Cova *et al.*[17] studied the timing limitations using channel plate detectors. Using a 1 GHz preamplifier will add approximately 10 ps in timing uncertainty due to electronic circuit noise. Furthermore, the transient time spread of channel plate detectors is less than 50 ps.[18] Thus the total time resolution of an instrument equipped with this detector should be better than 100 ps.

This result is obtained for channel plates with an active area of 40 mm diam and a pore size of 25 μm. A significant improvement of the rise time and the pulse width is anticipated for channel plates with a smaller pore size, since rise time and pulse width roughly scale with the pore size of the channel plates.[18] As a comparison with other solutions, the high-speed detector from Galileo has a rise time of "less than a nanosecond" and a pulse width "typically of one nanosecond" with a pore size of 12 μm and 20 mm diam active area;[8] the high-speed detector from Hamamatsu has a rise time of 250 ps and a pulse width of 600 ps with 6 μm pore size and 18 mm diam active area.[9]

ACKNOWLEDGMENTS

The authors are grateful to J. Fischer, H. Hofstetter, and R. Liniger for their contributions in the areas of design, fabrication, and electronics, respectively, and to W. Amacher and M. Wüthrich from the Institut für Angewandte Physik, University of Bern, for the loan of their HF equipment. This work was supported by the Swiss National Science Foundation.

APPENDIX A: IMPEDANCE ALONG TRANSITION LINE

In this section we present the proof that the line impedance is constant along the transition line. In analogy to the theoretical treatment given in Ref. 11, we first calculate the capacitance per unit length C_u and from that derive the line impedance by $Z_L=1/(C_u v)$, where v is the phase velocity. The electric field lines are given by a family of circles perpendicular to the circles of Apollonius, and go through the points P'. The centers of these circles are located on the y axis at the position M'_x (see Fig. 5) and we can make the following substitution:

$$Z_L=\frac{1}{2\pi}\frac{\sqrt{\mu_0\mu_r}}{\sqrt{\epsilon_0\epsilon_r}}\int_{\vec{s}(G_2)}^{\vec{s}(G_1)}\frac{1}{\vec{s}}d\vec{s}$$

$$=\frac{1}{2\pi}\frac{\sqrt{\mu_0\mu_r}}{\sqrt{\epsilon_0\epsilon_r}}\int_{\varphi(G_2)}^{\varphi(G_1)}\frac{1}{r_x\sin\varphi}r_x\,d\varphi, \tag{A1}$$

with the points G_1 and G_2, a function of M'_x and r_x the radius of the electric field line. Thus the impedance along the transition line is

$$Z_L(y)=Z_L(M'_x)=60\ \Omega\log\left(\frac{\tan[(\varphi_0-\varphi_1)/2]}{\tan[(\varphi_2-\varphi_3)/2]}\right), \tag{A2}$$

with φ_0, φ_1, φ_2, and φ_3 defining the start and the stop of the integration, which are all functions of M'_x. For the cable side of the transition line the numerator of the logarithmic term can be expanded to

$$\tan\left(\frac{\varphi_0-\varphi_1}{2}\right)=\frac{\sin\varphi_0\cos\varphi_1-\cos\varphi_0\sin\varphi_1}{1+\cos\varphi_0\cos\varphi_1+\sin\varphi_0\sin\varphi_1} \tag{A3}$$

and the denominator to

$$\tan\left(\frac{\varphi_2-\varphi_3}{2}\right)=\frac{\sin\varphi_2\cos\varphi_3-\cos\varphi_2\sin\varphi_3}{1+\cos\varphi_2\cos\varphi_3+\sin\varphi_2\sin\varphi_3}. \tag{A4}$$

With reference to Fig. 5, the angles φ_0, φ_1, φ_2, and φ_3 can be substituted with the following expressions:

$$\varphi_0=\arccos\left(\frac{M'_x}{\sqrt{M'^2_1+M'^2_x}}\right)=\arcsin\left(\frac{M'_1}{\sqrt{M'^2_1+M'^2_x}}\right), \tag{A5}$$

$$\varphi_1=\arccos\left(\frac{M'^2_x+P'^2}{\sqrt{M'^2_1+M'^2_x}}\right)=\arcsin\left(\frac{r'_1}{\sqrt{M'^2_1+M'^2_x}}\right), \tag{A6}$$

$$\varphi_2=\arccos\left(\frac{M'_x}{\sqrt{M'^2_2+M'^2_x}}\right)=\arcsin\left(\frac{M'_2}{\sqrt{M'^2_2+M'^2_x}}\right), \tag{A7}$$

$$\varphi_3=\arccos\left(\frac{\sqrt{P'^2+M'^2_x}}{\sqrt{M'^2_2+M'^2_x}}\right)=\arcsin\left(\frac{r'_2}{\sqrt{M'^2_2+M'^2_x}}\right). \tag{A8}$$

Inserting Eqs. (A5) through (A8) into Eqs. (A3) and (A4) gives

$$\frac{\tan[(\varphi_0-\varphi_1)/2]}{\tan[(\varphi_2-\varphi_3)/2]}=\frac{(M'_1\sqrt{M'^2_x+P'^2}-M'_x r'_1)(M'^2_2+M'^2_x+M'_x\sqrt{M'^2_x+P'^2}+M'_2 r'_2)}{[(M'^2_1+M'^2_x)+M'_x\sqrt{M'^2_x+P'^2}+M'_1 r'_1](M'_2\sqrt{M'^2_x+P'^2}-M'_x r'_2)}. \tag{A9}$$

To prove that the impedance is constant over the entire length of the transition line, this expression has to be independent from M'_x. To eliminate the variables M'_1, M'_2, r'_2, and P' we insert Eqs. (6) through (9) into Eq. (A9). This reduces the number of variables to the three defining parameters A', C', and r'_1 (see theory section). After some algebraic manipulations Eq. (A9) simplifies to

$$\frac{\tan[(\varphi_0-\varphi_1)/2]}{\tan[(\varphi_2-\varphi_3)/2]}=\frac{C'}{A'}. \tag{A10}$$

Thus, the line impedance is given as

$$Z_L=60\ \Omega\sqrt{\frac{\mu_r}{\epsilon_r}}\log\left(\frac{C'}{A'}\right). \tag{A11}$$

Since no dependence on M'_x is found, the impedance is constant along the transition line from the cable side to the points (T_1,T_2), which is the place where the two sets of families of circles connect.

In a similar way we define for the anode side of the transition line the angles φ_5, φ_6, φ_7, and φ_8 as the limits of integration (see Fig. 5). We then get for the argument of the logarithm

$$\frac{\tan[(\varphi_5+\varphi_6)/2]}{\tan[(\varphi_7+\varphi_8)/2]}=\frac{(M''^2_2+M''^2_x+M''_x\sqrt{M''^2_x-P''^2})(M''_1\sqrt{M''^2_x-P''^2}+M''_x r''_1)}{(M''_x\sqrt{M''^2_x-P''^2}+M''^2_x+M''^2_1)(M''_2\sqrt{M''^2_x-P''^2})}. \tag{A12}$$

Again, after some manipulations we get for the line impedance of the transition line from the anode side to the points (T_1,T_2)

$$Z_L=60\ \Omega\sqrt{\frac{\mu_r}{\epsilon_r}}\log\left(\frac{C''}{A''}\right). \tag{A13}$$

In all cases—at the cable side, at the anode side, and through the transition line—ideal matching of the impedance to transmission line is achieved. There is no unsteadiness along the entire transmission of the signal from the anode to the 50 Ω cable. The impedance is also independent of the choice of r'_1 and r''_1, which allows for many different shapes of transition lines in bipolar geometry.

APPENDIX B: TRANSITION TO DIELECTRIC MEDIUM

According to Eq. (1), the ratio of the inner and outer diameter of a coaxial line changes when a dielectric medium is used, which is the case where the transition finally yields into the SMA connector. In our design we only reduce the diameter of the inner conductor to account for the effect of the dielectric medium (see Fig. 6) and keep the outer conductor at the same size. Again we wanted to have a smooth transition from the coaxial line in vacuum to a coaxial line filled with a dielectric medium.

Let the two shapes of the inner conductor and the boundary of the dielectric medium at the transition be given by the functions $y_1(z)$ and $y_2(z)$ along the axis of the line, z. If we insert this into Eq. (A1) and perform the integration from the inner conductor through the vacuum and through the dielectric to the outer conductor we obtain

$$\frac{50}{60}=\log y_2(z)-\log y_1(z)+\frac{1}{\sqrt{\epsilon_r}}\log D_2-\frac{1}{\sqrt{\epsilon_r}}\log y_2(z). \tag{B1}$$

Let us assume that the two functions $y_1(z)$ and $y_2(z)$ have the following form:

$$Y_1(z)=d_1 f_1(z) \quad \text{and} \quad Y_2(z)=d_1 f_2(z). \tag{B2}$$

Inserting these into Eq. (B1) gives

$$0=-\log f_1(z)+\left(1-\frac{1}{\sqrt{\epsilon_r}}\right)\log f_2(z) \tag{B3}$$

and finally

$$f_1(z)=f_2(z)^{[1-(1/\sqrt{\epsilon_r})]}. \tag{B4}$$

Equation (B4) leaves quite some freedom for the design of a transition from a coaxial line in vacuum to a coaxial line filled with a dielectric medium, with the only restriction being the maintenance of the outer diameter of the line.

[1] G. Gloeckler and K. C. Hsieh, Nucl. Instrum. Methods **165**, 537 (1979).
[2] D. C. Hamilton, G. Gloeckler, F. M. Ipavich, R. A. Lundgren, R. B. Sheldon, and D. Hovestadt, Rev. Sci. Instrum. **61**, 3104 (1990).
[3] E. Möbius, P. Bochsler, A. G. Ghielmetti, and D. C. Hamilton, Rev. Sci. Instrum. **61**, 3609 (1990).
[4] L. Gubler, E. Möbius, and P. Bochsler, Helv. Phys. Acta **66**, 429 (1993).
[5] L. Gubler, Ph.D. thesis, University of Bern, 1994.
[6] H. Rothard, K. Kroneberger, A. Clouvas, E. Veje, P. Lorenzen, N. Keller, J. Kemmler, W. Meckbach, and K.-O. Groeneveld, Phys. Rev. A **41**, 2521 (1990).
[7] M. A. Gruntman and V. A. Morozov, J. Phys. E **15**, 1356 (1982).
[8] Galileo Electro-Optics Corporation, Data Sheet No. 70, Sturbridge, MA, USA (1988).
[9] Hamamatsu Photonics, Technical Information, Sept. 1991.
[10] J. L. Wiza, Nucl. Instrum. Methods **162**, 587 (1979).
[11] O. Zinke and H. Brunswig, *Lehrbuch der Hochfrequenztechnik*, 2nd ed. (Springer, Berlin, 1973), Vol. 1.
[12] H. Meinke and A. Scheubner, Fernmelde technische zeitschrift, FTZ, **5**, 109 (1952).
[13] G. Beck, Rev. Sci. Instrum. **47**, 849 (1976).
[14] H. S. M. Coxeter, *Introduction to Geometry* (Wiley, New York, 1961).
[15] A. Ess, Ph.D. thesis, ETH Zürich, Switzerland, 1951.
[16] B. A. Dahlman, RCA Rev. **15**, 238 (1954).
[17] S. Cova, M. Ghioni, and F. Zappa, Rev. Sci. Instrum. **62**, 2596 (1991).
[18] H. Kume, K. Koyama, K. Nakatsugawa, S. Suzuki, and D. Fatlowitz, Appl. Opt. **27**, 1170 (1988).